Quantum Mechanical ab Initio Studies of the Structures and Stabilities of Halogen Azides XN_3 (X = F, Cl, Br, I)

M. Otto, S. D. Lotz,† and G. Frenking*

Fachbereich Chemie, Philipps-Universität Marburg, Hans-Meerwein-Strasse, D-3550 Marburg, Germany

Received January 9, 1992

We report theoretically predicted geometries, heats of formation, $X–N_3$ bond energies, and vibrational spectra of the halogen azides XN_3 (X = F, Cl, Br, I) and HN_3 calculated by quantum chemical methods at the Hartree–Fock and correlated levels using all-electron wave functions and effective-core potentials. The theoretical data are used to predict the geometries of BrN_3 and IN_3, which have experimentally not been measured yet. A trans-bent (C_s) geometry is calculated for the halogen azides with a nearly constant bond angle of ~172° for the N_3 unit. The XNN angle increases from ~103° for FN_3 to ~111° for IN_3. A partial reassignment of the experimental vibrational spectra of BrN_3 and IN_3 is suggested. The calculated $X–N_3$ bond strengths indicate the order H ≫ F > Cl > Br > I; i.e., FN_3 is predicted to have the strongest X–N bond among the halogen azides. The opposite stability order F < Cl < Br < I is calculated for the $XN–N_2$ bond of XN_3; i.e., the dissociation of XN_3 into XN ($^3\Sigma^-$) + N_2 is most exothermic for FN_3 but endothermic for IN_3. The theoretical results for the heat of formation and the $H–N_3$ and $HN–N_2$ dissociation energies are in excellent agreement with experimental results. The electronic structure of the halogen azides is analyzed with the help of the topological analysis of the wave function. The X–N bond is essentially a single bond with a polarity $X^{\delta-}–N^{\delta+}$ for FN_3 and $X^{\delta+}–N^{\delta-}$ for ClN_3, BrN_3, and IN_3. The covalent bond order index P_{AB} indicates that the $N_1–N_2$ bond in XN_3 is intermediate between a single and a double bond and that the $N_2–N_3$ bond has nearly a triple bond. The partial charge is always slightly negative at N_2 and slightly positive at N_3.

Introduction

Although halogen azides XN_3 (X = F, Cl, Br, I) have been known since the beginning of this century[1] and have been recognized as versatile compounds in synthetic chemistry, the study and usage of them has been hampered by their unpleasant tendency to explode violently. Dehnicke and co-workers[2–4] developed experimental techniques which allow the preparation of very pure IN_3, BrN_3, and ClN_3, but knowledge about the structures and reactivities of halogen azides is still very scarce.

The most explosive member of this class of compounds is probably fluorine azide, FN_3. Only very recently have the results of a complete structural and spectroscopic investigation of FN_3 been reported by Christen et al.[5] These authors presented besides their microwave and infrared spectra also the results of ab initio calculations on FN_3 at the Hartree–Fock and correlated level of theory.[5] Parallel to their work, theoretical studies of FN_3 were published by Peters et al.[6] Prior to these studies, only some theoretical calculations of structural parameters[7] and argon-matrix IR frequencies of few of the fundamental vibrations[8] were known.

For the next highest member of this family, ClN_3, the experimentally determined UV,[9] microwave,[10] and vibrational[11] spectra are available. Quantum mechanical calculations of ClN_3 at the Hartree–Fock level have been published by several groups.[12] The UV spectra[9] and vibrational frequencies[8,13] are reported for BrN_3 and IN_3, but the geometries of the two molecules are not known. No theoretical studies of BrN_3 and IN_3 are known to us.

In this paper we report the results of the first quantum mechanical study of all halogen azides XN_3 (X = F, Cl, Br, I). We have calculated the equilibrium geometries and vibrational spectra of the four molecules. For comparative reasons, we also present results for HN_3, for which experimental[14,15] and theoretical data[16,17] are available. We estimate theoretically the $X–N_3$ bond strength relative to $H–N_3$, and we discuss the thermodynamic stabilities of the calculated azides. The theoretical studies were performed at the Hartree–Fock and correlated level of theory, using Møller–Plesset perturbation theory to estimate the correlation energy. All-electron basis sets of different sizes as well as effective-core potentials (ECP) were employed, and the results

† Present address: Institut für Anorganisch und Analytische Chemie, Freie Universität Berlin, D-1000 Berlin 33, Germany.

(1) IN_3: Hantzsch, A.; Schümann, M. *Ber. Dtsch. Chem. Ges.* **1900**, *33*, 522. BrN_3: Spencer, D. A. *J. Chem. Soc.* **1925**, *127*, 217. ClN_3: Raschig, F. *Ber. Dtsch. Chem. Ges.* **1908**, *41*, 4194.
(2) (a) Dehnicke, K. *Angew. Chem.* **1976**, *88*, 612; *Angew. Chem., Int. Ed. Engl.* **1976**, *15*, 553. (b) Dehnicke, K. *Angew. Chem.* **1979**, *91*, 527; *Angew. Chem., Int. Ed. Engl.* **1979**, *18*, 500.
(3) Dehnicke, K.; Ruschke, P. Cited in ref 9.
(4) Dehnicke, K. *J. Inorg. Nucl. Chem.* **1965**, *27*, 809.
(5) Christen, D.; Mack, H. G.; Schatte, G.; Willner, H. *J. Am. Chem. Soc.* **1988**, *110*, 707.
(6) Peters, N. J. S.; Allen, L. C.; Firestone, R. A. *Inorg. Chem.* **1988**, *27*, 755.
(7) Clidewell, Ch.; Holden, H. D. *J. Mol. Struct.* **1982**, *90*, 131.
(8) Milligan, D. E.; Jacox, M. E. *J. Chem. Phys.* **1964**, *40*, 2461.
(9) Dehnicke, K.; Ruschke, P. *Z. Naturforsch.* **1978**, *33b*, 750.
(10) Cook, R. L.; Gerry, M. C. L. *J. Chem. Phys.* **1970**, *53*, 2525.
(11) Kollitsch, W. Ph.D. Thesis, Universität Marburg, 1974.
(12) (a) Destro, R.; Merati, F.; Ortoleva, E. *Chem. Phys. Lett.* **1988**, *145*, 193. (b) Klaeboe, P.; Nielsen, C. J.; Priebe, H.; Schei, S. H.; Sjøgren, C. E. *J. Mol. Struct.* **1986**, *141*, 161. (c) Langhoff, S. R.; Jaffe, R. L.; Chong, D. P. *Int. J. Quantum Chem.* **1983**, *23*, 875.
(13) Engelhardt, U.; Feuerhahn, M.; Minkwitz, R. *Z. Anorg. Allg. Chem.* **1978**, *440*, 210.
(14) (a) Winnewisser, B. P. *J. Mol. Spectrosc.* **1980**, *82*, 220. (b) Moore, C. B.; Rosengreen, K. J. *J. Chem. Phys.* **1964**, *40*, 2461. (c) Foy, B. R.; Casassa, M. P.; Stephenson, J. C.; King, D. S. *J. Chem. Phys.* **1988**, *89*, 608. (d) Kajimoto, O.; Yamamoto, T.; Fueno, T. *J. Phys. Chem.* **1979**, *83*, 429. (e) Richardson, W. C.; Setser, D. W. *Can. J. Chem.* **1969**, *47*, 2725.
(15) Milligan, D. E.; Jacox, M. E. *J. Chem. Phys.* **1964**, *41*, 2839.
(16) (a) Alexander, M. H.; Werner, H.-J.; Dagdigian, P. J. *J. Chem. Phys.* **1988**, *89*, 1388. (b) Nielsen, C. J.; Sjøgren, C. E. *THEOCHEM* **1987**, *150*, 361. (c) Sjøgren, C. E.; Nielsen, C. J. *J. Molec. Struct.* **1986**, *142*, 285.
(17) (a) Lievin, J.; Breulet, J.; Verhaegen, G. *Theoret. Chim. Acta* **1981**, *60*, 339. (b) Breulet, J.; Lievin, J. *Theoret. Chim. Acta* **1982**, *61*, 59. (c) Lievin, J.; Breulet, J.; Verhaegen, G. *Theoret. Chim. Acta* **1979**, *52*, 75. (d) Kahn, S. D.; Hehre, W. J.; Pople, J. A. *J. Am. Chem. Soc.* **1987**, *109*, 1871. (e) Sana, M.; Leroy, G.; Nguyen, M.-T.; Elguero, J. *Nouv. J. Chim.* **1979**, *3*, 607. (f) Murgich, J.; Aray, Y. *J. Chem. Phys.* **1987**, *87*, 3580. (g) Dewar, M. J. S.; Storch, D. M. *J. Am. Chem. Soc.* **1985**, *107*, 3898. (h) Ibrahim, M. R.; Schleyer, P. v. R. *J. Comput. Chem.* **1985**, *6*, 157. (i) Levin, A.; Leroux, J. P.; Bigot, B.; Devaquet, A. *Chem. Phys. Lett.* **1980**, *45*, 305.

0020-1669/92/1331-3647$03.00/0

of the different procedures are compared with each other. Thus, our study may be used to judge the quality of the ECP approach relative to all-electron basis sets. Details of the theoretical methods are described below.

The electronic structures of the geometry-optimized molecules are analyzed using the topological theory of atoms in molecules.[18-21] Very recently, a partitioning scheme has been suggested which defines covalent bond orders in the framework of the topological theory of atoms in molecules.[22]

Theoretical Details

The calculations have been performed using the program packages Gaussian 90[23] and CADPAC.[24] The following basis sets have been employed for the all-electron calculations. For HN_3, FN_3, and ClN_3, we used the standard 3-21G(d,p)[25] and 6-31G(d,p)[26] basis sets with six d-functions for the heavy atoms and three p-functions for H. Note that the 3-21G(d,p) basis sets has the same exponents for the p- and d-polarization functions as 6-31G(d,p). In case of BrN_3 and IN_3, we used for Br and I the basis sets suggested by Huzinaga,[27] which are split for Br (43321|4321|41) and for I (433321|43321|431). These basis sets, which are intermediate in quality between 3-21G and 6-31G, have been augmented by a set of six d-functions. They are denoted HUZ(d). The exponents for the polarization functions are H (1.1), N (0.8), F (0.8), Cl (0.514), Br (0.389), I (0.266). Open-shell molecules are treated with the unrestricted Hartree–Fock (UHF) method. We also performed all-electron calculations for the halogen azides including correlation energy using Møller–Plesset perturbation theory terminated at second order.[28] The optimizations and frequency calculations have been carried out at MP2/6-31G(d,p), with the Huzinaga basis sets for Br and I.

We also carried out ECP calculations utilizing the parameters developed by Hay and Wadt,[29] which are implemented in Gaussian 90 and termed LANL1DZ. The LANL1DZ model uses all-electron wave functions for hydrogen and first-row elements and ECPs for heavier atoms, in our case Cl, Br, and I. The basis functions for the valence s and p electrons consist of the standard double-ζ basis set as developed by Huzinaga[30a,b] and Dunning.[30c,d] As a next step, we added a set of five d-type polarization functions (three p-functions at H). This level of theory is denoted as LANL1DZ+P. We also optimized the structures and calculated the vibrational spectra using ECPs with inclusion of correlation energy at the MP2/LANL1DZ+P level.

For the calculation of the open-shell molecules the spin-unrestricted (UHF) method was used. In order to give more reliable estimates of the reaction energies involving open-shell species, techniques of spin-projection[31] were used which eliminate some (but not all) contributions from higher spin states. We present the calculated eigenvalues $\langle S^2 \rangle$ of the S^2 operator and the energies of the spin-projected wave functions at the MP2 level, i.e. PMP2/6-31G(d,p) and PMP2/LANL1DZ+P.

The analysis of the electron density distribution and the calculation of $\nabla\rho(\mathbf{r})$ and $\nabla^2\rho(\mathbf{r})$ was carried out using the programs PROAIM and SADDLE.[32] The covalent bond orders have been computed using the program BONDER.[33]

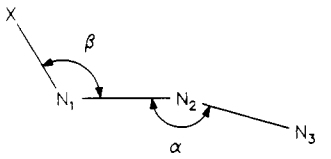

Figure 1. Schematic representation of the geometry of XN_3 molecules.

Results and Discussion

1. Geometries. The experimentally determined geometries of HN_3,[14a] FN_3,[5] and ClN_3[10] exhibit a trans-bent (C_s) structure with only a slight deviation of the N_3 unit from linearity (Figure 1).

Table I shows the calculated geometries at various levels of theory and the experimentally observed bond lengths and bond angles, as far as they are available. The results obtained by the all-electron calculations are very similar to the geometries using ECP wave functions at a comparable level of theory. That is, the HF/6-31G(d,p) geometries are not very different from the HF/LANL1DZ+P structures, and the same holds true for geometries predicted at MP2/6-31G(d,p) and MP2/LANL1DZ+P (Table I). This is particularly noteworthy for the I–N bond length, since the ECPs have been developed with inclusion of relativistic effects, while the all-electron calculations reported here do not include relativistic terms. The addition of polarization functions to the LANL1DZ basis set yields significant changes in the calculated geometries, while the HF/3-21G(d) and HF/6-31G(d,p) optimized structures show less alterations. The interatomic distances become larger at the correlated level, but the bond angles change only slightly.

All calculated XN_3 molecules are predicted by theory with a trans-bent geometry. The N_3 unit is calculated at the correlated level with a bond angle α of about 172°, independent of the nature of X. The XNN angle β increases regularly from ~103° for FN_3 to ~111° for IN_3 (Table I) following the trend predicted by Bent's rule, which states that substitutents with higher electronegativity change the hybridization towards more p-character, thus yielding smaller bond angles. The agreement between theoretically predicted and experimentally observed bond lengths based on the MP2 results is good for the X–N distances but less satisfactory for the N_1–N_2 and N_2–N_3 bond lengths. It should be noted that a high theoretical level is necessary for a good description of bonds between electronegative atoms; a particular difficult molecule is F_2O_2.[34] The theoretical results shown in Table I let us predict that BrN_3 and IN_3 have trans-bent geometries with slightly larger values for the angle β than found for ClN_3 and the same value for α. The X–N distance should be close to 1.92 Å for Br–N_3 and 2.11 Å for I–N_3.

2. Vibrational Spectra. The theoretically predicted vibrational frequencies for XN_3 molecules have been calculated with the harmonic approximation. The deviation from the experimentally obtained frequencies may partly be compensated by using scaling

(18) Bader, R. F. W. *Atoms in Molecules. A Quantum Theory*; Oxford Press: Oxford, England. 1990.
(19) (a) Bader, R. F. W.; Tal, Y.; Anderson, S. G.; Nguyen-Dang, T. T. *Isr. J. Chem.* **1980**, *19*, 8. (b) Bader, R. F. W.; Nguyen-Dang, T. T.; Tal, Y. *Rep. Prog. Phys.* **1981**, *44*, 893. (c) Bader, R. F. W.; Nguyen-Dang, T. T. *Adv. Quantum Chem.* **1981**, *14*, 63.
(20) (a) Bader, R. F. W.; Slee, T. S.; Cremer, D.; Kraka, E. *J. Am. Chem. Soc.* **1983**, *105*, 5061. (b) Bader, R. F. W.; MacDougall, P. J. *J. Am. Chem. Soc.* **1985**, *107*, 6788.
(21) Cremer, D.; Kraka, E. *Angew. Chem.* **1984**, *96*, 612; *Angew. Chem., Int. Ed. Engl.* **1984**, *23*, 627.
(22) Cioslowski, J.; Mixon, S. T. *J. Am. Chem. Soc.* **1991**, *113*, 4142.
(23) Gaussian 90: Frisch, M. J.; Head-Gordon, M.; G. W. Trucks, G. W.; Foreman, J. B.; Schlegel, H. B.; Raghavachari, K.; Robb, M. A.; Binkley, J. S.; Gonzalez, C.; DeFrees, D. J.; Fox, D. J.; Whiteside, R. A.; Seeger, R.; Melius, C. F.; Baker, I.; Martin, R.; Kahn, L. R.; Stewart, J. J. P.; Topiol, S.; Pople, J. A. Gaussian Inc., Pittsburgh, PA 1990.
(24) Amos, R. D.; Rice, J. E.: CADPAC: The Cambridge Analytical Derivatives Package, issue 4.0. Cambridge, 1987.
(25) (a) Binkley, J. S.; Pople, J. A.; Hehre, W. J. *J. Am. Chem. Soc.* **1980**, *102*, 939. (b) Gordon, M. S.; Binkley, J. S.; Pople, J. A.; Pietro, W. J.; Hehre, W. J. *J. Am. Chem. Soc.* **1982**, *104*, 2797. (c) Pietro, W. J.; Francl, M. M.; Hehre, W. J.; DeFrees, D. J.; Pople, J. A.; Binkley, J. S. *J. Am. Chem. Soc.* **1982**, *104*, 5039.
(26) (a) Ditchfield, R.; Hehre, W. J.; Pople, J. A. *J. Chem. Phys.* **1971**, *54*, 724. (b) Hehre, W. J.; Lathan, W. A. *J. Chem. Phys.* **1972**, *56*, 5255.
(27) Andzelm, J.; Huzinaga, S.; Klobukowski, M.; Radzio, E.; Sakai, Y.; Tatekawi, H. *Gaussian Basis Sets for Molecular Calculations*; Elsevier: Amsterdam, 1984.
(28) (a) Møller, C.; Plesset, M. S. *Phys. Rev.* **1934**, *46*, 618. (b) Binkley, J. S.; Pople, J. A. *Int. J. Quantum Chem.* **1975**, *9*, 229.
(29) Hay, P. J.; Wadt, W. R. *J. Chem. Phys.* **1985**, *82*, 270, 284, 299.
(30) (a) Huzinaga, S. *J. Chem. Phys.* **1965**, *42*, 1293. (b) Huzinaga S.; Saki, Y. *J. Chem. Phys.* **1969**, *50*, 1371. (b) Dunning, T. H. *J. Chem. Phys.* **1970**, *53*, 2823. (d) Dunning, T. H.; Hay, P. J. In *Modern Theoretical Chemistry*; Schaefer, H. F., Ed.; Plenum Press: New York, 1977; Vol. 3, Chapter 1.
(31) (a) Sosa, C.; Schlegel, H. B. *Int. J. Quantum Chem.* **1986**, *29*, 1001. (b) Schlegel, H. B. *J. Chem. Phys.* **1986**, *84*, 4530.
(32) Biegler-König, F. W.; Bader, R. F. W.; Ting-Hua, T. *J. Comput. Chem.* **1982**, *3*, 317.
(33) BONDER: Cioslowski, J. Florida State University, 1991.
(34) Rohlfing, C. M.; Hay, P. J. *J. Chem. Phys.* **1987**, *86*, 4518.

Table I. Optimized and Experimentally Observed Geometries with Distances in Å, Angles in deg, and Calculated Total Energies in Hartrees

	HF/3-21G(d,p)[b]	HF/6-31G(d,p)[b]	MP2/6-31G(d,p)[b]	HF/LANL1DZ	HF/LANL1DZ+P	MP2/LANL1DZ+P	exptl[a]
				HN_3			
$r(H-N_1)$	1.015	1.006	1.018	1.012	1.006	1.023	1.015
$r(N_1-N_2)$	1.238	1.238	1.250	1.273	1.247	1.266	1.243
$r(N_2-N_3)$	1.098	1.099	1.158	1.121	1.102	1.171	1.134
α	173.9	173.8	171.2	171.4	174.3	171.5	171.3
β	107.4	108.2	109.7	110.9	107.8	109.0	108.8
$E_{tot.}$	−163.0574	−163.8429	−164.3614	−163.7564	−163.8707	−164.3699	
				FN_3			
$r(F-N_1)$	1.381	1.382	1.431	1.450	1.383	1.441	1.444
$r(N_1-N_2)$	1.258	1.253	1.280	1.314	1.263	1.293	1.253
$r(N_2-N_3)$	1.098	1.110	1.152	1.115	1.103	1.161	1.132
α	173.8	174.0	171.7	175.3	174.7	172.4	170.9
β	104.2	104.3	103.8	102.7	104.2	103.3	103.8
$E_{tot.}$	−261.3451	−262.6025	−263.2824	−262.5335	−262.6606	−263.3103	
				ClN_3			
$r(Cl-N_1)$	1.741	1.734	1.753	1.863	1.742	1.767	1.745
$r(N_1-N_2)$	1.252	1.247	1.265	1.300	1.257	1.278	1.252
$r(N_2-N_3)$	1.096	1.098	1.157	1.117	1.102	1.167	1.133
α	173.6	174.1	171.3	173.6	174.7	171.7	171.9
β	108.5	109.0	109.3	107.8	108.3	108.1	108.6
$E_{tot.}$	−619.8430	−622.6894	−623.3416	−177.8222	−177.9528	−178.5733	
				BrN_3			
$r(Br-N_1)$	1.908	1.896	1.923	1.992	1.891	1.919	
$r(N_1-N_2)$	1.248	1.244	1.262	1.287	1.251	1.274	
$r(N_2-N_3)$	1.096	1.098	1.160	1.120	1.103	1.170	
α	174.0	174.2	171.4	173.3	174.8	171.9	
β	108.1	109.1	108.5	110.6	109.8	109.4	
$E_{tot.}$	−2732.5896	−2733.6089	−2734.0035	−174.0580	−176.1829	−176.7946	
				IN_3			
$r(I-N_1)$	2.112	2.090	2.120	2.120	2.058	2.095	
$r(N_1-N_2)$	1.292	1.238	1.255	1.274	1.245	1.268	
$r(N_2-N_3)$	1.102	1.099	1.165	1.124	1.104	1.175	
α	172.4	174.4	171.6	173.1	174.8	171.8	
β	109.5	111.4	110.4	114.5	112.3	111.2	
$E_{tot.}$	−7075.3544	−7076.2957	−7076.9339	−174.3006	−174.4187	−175.0188	

[a] Exptl data: HN_3, ref 14a; FN_3, ref 5; ClN_3, ref 10. [b] HUZ(d) for Br and I.

factors which change at different theoretical levels.[35] They may also be different for the various vibrational modes which are present in the molecule. The calculated frequencies are usually too high, but sometimes they may be smaller than the experimental values.[35] But it should also be noted that the experimentally observed frequencies may change substantially when measured under different conditions. Table II shows our calculated vibrational frequencies, IR intensities, and Raman activities in comparison with the experimental results.

For all four halogen azides, the highest normal mode frequency ν_1 corresponds to the N_3 asymmetric stretching mode, which is rather independent of the nature of X. The experimental frequencies ν_1 for the halogen azides are between 2037 and 2075 cm^{-1} (Table II). The MP2 frequencies are uniformly too high by a factor of ~1.15. The calculations predict that ν_1 should have the highest intensity in the IR spectra, which is in agreement with experimental results (Table II).

The next highest lying frequency ν_2 corresponds to the symmetric N_3 stretching mode which increases from 1090 cm^{-1} (FN_3) to 1240 cm^{-1} (IN_3). ν_2 is a case where the experimental value is strongly dependent on the experimental conditions. For IN_3, ν_2 is reported as 1240 cm^{-1} when it is measured in Nujol but at 1176 cm^{-1} when it is measured in benzene.[2a] The computed frequencies for ν_2 of XN_3 are too high by an average factor of 1.03 (MP2 level), but otherwise they agree quite well with the experimental data.

As expected, the vibrational frequency for the X–N stretching mode decreases from F to I (Table II). For FN_3, ClN_3, and BrN_3, the MP2 frequencies are too high by a factor of ~1.05. The same factor is found when the MP2 values for the I–N stretching mode (426 and 429 cm^{-1}) are compared with the experimental values reported by Engelhardt et al.[13] (400 and 410 cm^{-1}). A much lower I–N frequency (338 cm^{-1}) has been reported by Dehnicke,[2a] who noted the unusually low value. Engelhardt et al.[13] found also a band at 338 cm^{-1} in the Raman spectrum, but they attributed the signal to solid iodine acid. Our calculated data support the assignment of Engelhardt et al.[13] for the I–N stretching mode in IN_3 at 400–410 cm^{-1}.

The only other normal mode which is reported for all halogen azids is the deformation mode $\delta(N_3)$ which increases from 241 cm^{-1} for FN_3 to 578–648 cm^{-1} for IN_3 (Table II). Our theoretically predicted data suggest that the assignments of the experimentally observed vibrational modes may not always be correct. The MP2 frequencies for the $\delta(N_3)$ mode of FN_3 and ClN_3 are too high by a factor of ~1.04 (Table II). The same factor is calculated for IN_3 if the experimental value of Dehnicke[2a] (648 cm^{-1}) is used. Engelhardt et al.[13] report much lower values of 583 and 595 cm^{-1}. However, these authors noted already uncertanties concerning the assignments of the $\delta(N_3)$ and $\gamma(N_3)$ mode. The calculated values suggest that the assignments of the vibrational frequencies for the $\delta(N_3)$ and $\gamma(N_3)$ modes of IN_3 reported by Engelhardt et al.[13] should be reversed; i.e., the values of 583 (Raman) and 595 cm^{-1} (IR) correspond to the $\gamma(N_3)$ mode and the frequencies found at 623 and 628 cm^{-1} correspond to the $\delta(N_3)$ mode. As shown below, this is also in better agreement with our calculated values for the $\gamma(N_3)$ mode of XN_3 molecules. We also question the assignment for the frequency at 530 cm^{-1} to the $\delta(N_3)$ mode of BrN_3 by Milligan and Jacox.[8] With application of the same scaling factor of 1.04, the $\delta(N_3)$ mode should appear at ~465 cm^{-1}. The experimentally observed

(35) Hehre, W. J.; Radom, L.; Schleyer, P. v. R.; Pople, J. A. *Ab Initio Molecular Orbital Theory*; Wiley: New York, 1986; p 236 f.

Table II. Calculated Vibrational Frequencies (cm^{-1}), IR Intensities (km/mol), and Raman Intensities ($Å^4$/amu) and Experimentally Observed Frequencies

HN_3

	HF/6-31G(d,p)	MP2/6-31G(d,p)	HF/LANL1DZ+P	MP2/LANL1DZ+P	exptl IR[a]	assgnt
ν1 (A′)	3732	3585	3681	3573	3324	ν(H–N)
IR intensity	34	62	29	68	m	
Raman intensity	123	nc	nc	nc		
ν2 (A′)	2511	2391	2298	2350	2150	ν(N_3, asym)
IR intensity	555	198	489	203	vs	
Raman intensity	52	nc	nc	nc		
ν3 (A′)	1436	1267	1422	1237	1273	δ(N_3)
IR intensity	46	1	76	3	m	
Raman intensity	13	nc	nc	nc		
ν4 (A′)	1253	1130	1055	1135	1168	ν(N_3, sym)
IR intensity	271	209	296	190	vs	
Raman intensity	4	nc	nc	nc		
ν5 (A′)	574	551	506	541	527	δ(HNN)
IR intensity	19	28	17	29	w	
Raman intensity	1	nc	nc	nc		
ν6 (A″)	677	579	584	559	588	γ(N_3)
IR intensity	5	1	1	1	w	
Raman intensity	<1	nc	nc	nc		

FN_3

	HF/6-31G(d,p)	MP2/6-31G(d,p)	HF/LANL1DZ+P	MP2/LANL1DZ+P	exptl IR[b]	assgnt
ν1 (A′)	2386	2405	2354	2384	2037	ν(N_3, asym)
IR intensity	395	141	409	155	vs	
Raman intensity	66	nc	nc	nc		
ν2 (A′)	1225	1151	1266	1135	1090	ν(N_3, sym)
IR intensity	28	2	30	2	m	
Raman intensity	7	nc	nc	nc		
ν3 (A′)	1045	948	1029	928	873	ν(F–N)
IR intensity	176	42	210	51	s	
Raman intensity	10	nc	nc	nc		
ν4 (A′)	758	690	748	673	658	δ(FNN)
IR intensity	6	4	6	5	m	
Raman intensity	3	nc	nc	nc		
ν5 (A′)	282	247	283	245	241	δ(N_3)
IR intensity	5	5	5	5	m	
Raman intensity	4	nc	nc	nc		
ν6 (A″)	606	494	599	470	504	γ(N_3)
IR intensity	14	3	9	2	w	
	<1	nc	nc	nc		

ClN_3

	HF/6-31G(d,p)	MP2/6-31G(d,p)	HF/LANL1DZ+P	MP2/LANL1DZ+P	exptl IR[c]	exptl Ra[c]	assgnt
ν1 (A′)	2450	2382	2415	2359	2075	2066	ν(N_3, asym)
IR intensity	545	268	555	278	vs	w	
Raman intensity	126	nc	nc	nc			
ν2 (A′)	1237	1202	1202	1173	1140	1134	ν(N_3, sym)
IR intensity	158	27	165	25	s	w	
Raman intensity	9	nc	nc	nc			
ν3 (A′)	818	757	816	761	719	719	ν(Cl–N)
IR intensity	41	11	45	8	m	m	
Raman intensity	29	nc	nc	nc			
ν4 (A′)	626	574	615	570	545	540	δ(N_3)
IR intensity	17	1	8	1	w	s	
Raman intensity	1	nc	nc	nc			
ν5 (A′)	248	212	246	209	223	221	δ(ClNN)
IR intensity	2	3	2	3	vw	s	
Raman intensity	7	nc	nc	nc			
ν6 (A″)	617	511	616	484	522	no[h]	γ(N_3)
IR intensity	7	4	11	2	w		
Raman intensity	24	nc	nc	nc			

BrN_3

	HF/6-31G(d,p)[i]	MP2/6-31G(d,p)[i]	HF/LANL1DZ+P	MP2/LANL1DZ+P	exptl IR[d]	assgnt
ν1 (A′)	2451	2348	2418	2330	2053, 2020	ν(N_3, asym)
IR intensity	615	342	657	369		
Raman intensity	162	nc	nc	nc		

Table II. (Continued)

	BrN_3					
	HF/6-31G(d,p)[i]	MP2/6-31G(d,p)[i]	HF/LANL1DZ+P	MP2/LANL1DZ+P	exptl IR[d]	assgnt
ν2 (A′)	1247	1208	1228	1190	1160	$\nu(N_3$, sym)
IR intensity	212	34	232	37		
Raman intensity	14	nc	nc	nc		
ν3 (A′)	774	712	769	708	687	ν(Br–N)
IR intensity	22	5	23	4		
Raman intensity	27	nc	nc	nc		
ν4 (A′)	520	478	520	493	530[e]	$\delta(N_3)$
IR intensity	4	1	3	2		
Raman intensity	39	nc	nc	nc		
ν5 (A′)	216	182	213	178	no[h]	δ(BrNN)
IR intensity	1	2	<1	2		
Raman intensity	8	nc	nc	nc		
ν6 (A″)	635	517	627	480	no[h]	$\gamma(N_3)$
IR intensity	16	4	11	<1		
Raman intensity	1	nc	nc	nc		

	IN_3							
	HF/6-31G(d,p)[i]	MP2/6-31G(d,p)[i]	HF/LANL1DZ+P	MP2/LANL1DZ+P	exptl IR[e]	exptl IR[f]	exptl Ra[f]	assignt
ν1 (A′)	2457	2307	2423	2291	2045, 2058	2050	2052	$\nu(N_3$, asym)
IR intensity	770	460	814	483	vs	vs	m	
Raman intensity	200	nc	nc	nc				
ν2 (A′)	2181	1228	1267	1209	1240, 1176	1222	1207	$\nu(N_3$, sym)
IR intensity	286	44	306	46	m	m	w	
Raman intensity	20	nc	nc	nc				
ν3 (A′)	747	679	743	676	648	595[g]	583[g]	$\delta(N_3)$
IR intensity	16	4	16	4	vw	w	w	
Raman intensity	32	nc	nc	nc				
ν4 (A′)	472	429	471	426	338	400	410	ν(I–N)
IR intensity	<1	<1	<1	<1	m	w	vs	
Raman intensity	60	nc	nc	nc				
ν5 (A′)	197	164	194	161	no[h]	no[h]	218	δ(INN)
IR intensity	1	2	1	2			w	
Raman intensity	10	nc	nc					
ν6 (A″)	649	524	640	500	580, 578	623[g]	628[g]	$\gamma(N_3)$
IR intensity	16	3	11	2	w	vw	vw	
Raman intensity	2	nc	nc	nc				

[a] Reference 14b. [b] Reference 5. [c] Reference 11. [d] Reference 8. [e] Assignment probably wrong; see text. [f] Reference 13. [g] Assignment probably wrong; see text. [h] Not observed. [i] HUZ(d) for Br and I.

frequency at 530 cm^{-1} fits much better with our calculated value for the $\gamma(N_3)$ mode (see below). The frequency for the δ(XNN) deformation mode is very low, with the exception of FN_3, and the calculated values at the MP2 level are in most cases smaller than the experimental values (Table II).

The calculated frequency for the out-of-plane vibration $\gamma(N_3)$ at the MP2 level is always too low by ~0.9–0.95 (Table II). The experimentally observed vibrational frequencies at 583 and 595 cm^{-1} for IN_3[13] and at 530 cm^{-1} for BrN_3[8] are therefore assigned by us to $\gamma(N_3)$ and not to $\delta(N_3)$ as originally suggested.[8,13]

3. Bond Strengths and Thermodynamic Stabilities of XN_3. The calculated total energies can be used to predict theoretically the binding energies and thermodynamic stabilities of the azides, which are difficult to determine experimentally. Of particular interest is the strength of the X–N_3 bond. We calculated the dissociation energies of reaction 1, which, after correction for

$$XN_3 \rightarrow N_3 + X + D_0 \qquad (1)$$

zero-point energies ZPE (scaled by 0.92[35]), differences in rotational and translational degrees of freedom (0.6 kcal/mol), and the work term (0.6 kcal/mol), are converted into dissociation enthalpies at room temperature D_0. The results are shown in Table III. The total energies and ZPE values for the fragments are given in Table IV.

Reaction 1 is predicted to be strongly exothermic, and the results are not very different between the ECP and the all-electron methods (Table III). The theoretically predicted bond strength for the H–N_3 bond is in very good agreement with the most recent experimental result by Illenberger et al.[36a] Because the spin contamination in the UHF wave function of N_3 is rather high ($\langle S^2 \rangle$ = 0.904 at MP2/6-31G(d,p) and 0.919 at MP2/LANL1DZ+P, theoretical value 0.75), the bond energies calculated at PMP2 are 5–10 kcal/mol smaller than the MP2 values.

The calculations predict that the X–N_3 bond strength decreases in the order H ≫ F > Cl > Br > I. The results that FN_3 has the strongest and IN_3 the weakest halogen–N_3 bond is surprising at first glance, since FN_3 is considered the least stable halogen azide, while IN_3 is the most stable.[1] However, thermal fragmentation of XN_3 is *not* induced by breaking the X–N_3 bond but rather by dissociation into XN and N_2. Since the electronic ground state of XN (X = halogen) is a ($^3\Sigma^-$) triplet state, dissociation of XN_3 (X^1A') into XN ($X^3\Sigma^-$) and N_2 ($X^1\Sigma^+_g$) is spin-symmetry forbidden. Nevertheless, pyrolysis experiments carried out in the temperature range of 285–470 °C has shown that HN_3 decomposes into N_2 and NH in the ground-state triplet ($X^3\Sigma^-$) state.[14e] A recently published theoretical study[16a] on the energetics of the dissociation reaction HN_3 (X^1A') → N_2 ($X^1\Sigma^+_g$) + HN ($X^3\Sigma^-$) at a very high level of theory using CASSCF and MCSCF-CI techniques has shown that singlet–triplet coupling occurs because the HN_3 wave function in the region of the transition

(36) (a) Illenberger, E.; Comita, P. B.; Brauman, J. I.; Fenzlaff, H.-P.; Heni, M.; Heinrich, N.; Koch, W.; Frenking, G. *Ber. Bunsen-Ges. Phys. Chem.* **1985**, *89*, 1026. (b) Gray, P. *Q. Rev.* (*London*) **1963**, *17*, 441.

Table III. Calculated Reaction Enthalpies D_0 (kcal/mol) for Reactions 1–3

	H	F	Cl	Br	I
		$XN_3 \rightarrow X^\bullet + N_3$ (1)			
MP2/6-31G(d,p)[a,b]	96.9 (87.4)	57.8 (47.7)	48.5 (38.3)	46.9 (36.8)	45.8 (35.6)
MP2/LANL1DZ+P	99.3 (94.8)	58.0 (52.9)	49.6 (44.3)	46.9 (41.6)	45.4 (40.3)
exptl	92.2 ± 4.6[c]				
	85[d]				
		$XN_3 \rightarrow N_2 + XN\ (^3\Sigma^-)$ (2)			
MP2/6-31G(d,p)[a,b]	+14.9 (+13.5)	−25.1 (−27.0)	−11.9 (−14.0)	−3.5 (−6.1)	+6.5 (+2.9)
MP2/LANL1DZ+P	+15.1 (+13.7)	−28.8 (−30.7)	−11.2 (−13.5)	−3.3 (−6.1)	+5.7 (+2.0)
exptl	17.5[e]				
	15.0[f]				
		$2XN_3 \rightarrow 3N_2 + X_2$ (3)			
MP2/6-31G(d,p)[a]	−144.2	−164.4	−185.6	−193.2	−191.4
MP2/LANL1DZ+P	−137.6	−157.8	−184.4	−184.6	−183.6

[a] MP2/HUZ(d) for Br and I. [b] Spin-projected (PMP2) results are given in parentheses. [c] Reference 36a. [d] Reference 36b. [e] Reference 14d. [f] Reference 37.

Table IV. Calculated Total Energies $E_{tot.}$ (Hartrees), Interatomic Distances r_{AB} (Å), and Zero-Point Vibrational Energies ZPE (kcal/mol)

	MP2/6-31G(d,p)[a]					MP2/LANL1DZ+P				
	$E_{tot.}$	$\langle s^2 \rangle$	$E_{tot.}$[b]	r_{AB}	ZPE	$E_{tot.}$	$\langle s^2 \rangle$	$E_{tot.}$[b]	r_{AB}	ZPE
N_2 ($^1\Sigma^+_g$)	−109.2616			1.130	2.9	−109.2638			1.139	2.8
HN ($^3\Sigma^-$)	−55.0707	2.014	−55.0729	1.035	4.5	−55.0769	2.014	−55.0791	1.038	4.5
FN ($^3\Sigma^-$)	−154.0584	2.019	−154.0614	1.329	1.6	−154.0830	2.020	−154.0860	1.342	1.6
ClN ($^3\Sigma^-$)	−514.0964	2.025	−514.0997	1.640	1.1	−69.3248	2.030	−69.3284	1.662	1.1
BrN ($^3\Sigma^-$)	−2624.7451	2.041	−2624.7493	1.806	1.0	−67.5336	2.045	−67.5381	1.808	1.0
IN ($^3\Sigma^-$)	−6967.6598	2.081	−6967.6655	2.005	0.9	−65.7437	2.082	−65.7496	1.981	0.9
H_2 ($^1\Sigma^+_g$)	−1.1577			0.734	6.1	−1.1576			0.733	6.1
F_2 ($^1\Sigma^+_g$)	−199.0388			1.421	1.3	−199.0775			1.429	6.1
Cl_2 ($^1\Sigma^+_g$)	−919.1912			2.015	0.7	−29.6461			2.023	0.7
Br_2 ($^1\Sigma^+_g$)	−5140.5278			2.309	0.5	26.0893			2.328	0.5
I_2 ($^1\Sigma^+_g$)	−13826.3859			2.716	0.3	−22.5367			2.699	0.5
N_3 ($^2\Pi$)	−163.6997	0.904	−163.7149	1.184	5.6	−163.7056	0.919	−163.7128	1.194	5.8
H• (^{2}S)	−0.4982					−0.4976				
F• (^{2}P)	−99.4890	0.753	−99.4900			−99.5111	0.753	−99.5121		
Cl• (^{2}P)	−459.5621	0.755	−459.5632			−14.7228	0.756	−14.7895		
Br• (^{2}P)	−2570.2285	0.756	−2570.2295			−13.0140	0.757	−13.0152		
I• (^{2}P)	−6913.1609	0.757	−6913.1620			−11.2411	0.757	−11.2421		

[a] MP2/HUZ(d) for Br and I. [b] Spin-projected energies.

state can be considered an equal mixture of N_2 (X)·NH ($a^1\Delta$) and N_2 (X)·NH ($b^1\Sigma^+$). The calculated barrier for the dissociation (35.7 kcal/mol) is in excellent agreement with the value $E_a \sim 36$ kcal/mol estimated from thermal dissociation studies in a shock tube.[14d]

This result suggests that the stabilities of XN_3 molecules may be determined by the activation barrier for breaking the XN–N_2 bond, which in turn involves singlet–triplet coupling along the reaction course. Because an accurate calculation of the dissociation barrier of XN_3 yielding XN and N_2 needs a very high level of theory which is not possible for larger atoms X at the present time, we calculated only the reaction energy of the corresponding reaction 2. The reaction energies are converted into

$$XN_3\ (X^1A') \rightarrow N_2\ (X^1\Sigma^+_g) + XN\ (X^3\Sigma^-) + D_0 \quad (2)$$

D_0 enthalpies at room temperature using the ZPE corrections (Table IV) and corrections for rotational and translational degrees of freedom (1.2 kcal/mol) and the work term pV (0.6 kcal/mol). The theoretically predicted results are shown in Table III.

The calculated reaction energies for reaction 2 show a stability for the halogen azides opposite to that which is predicted for reaction 1; i.e., FN_3 is now least stable and IN_3 is the most stable halogen azide. The theoretical values for the dissociation enthalpy of HN_3 (14.9 and 15.1 kcal/mol at MP2, 13.5 and 13.7 kcal/mol at PMP2; Table III) are in very good agreement with the experimental results of 15.0 kcal/mol by Melius[37] and 17.5 kcal/mol by Kajimoto et al.[14d] The PMP2 results are not very different from the MP2 values, because the spin contamination in the UHF wave functions of XN ($X^3\Sigma^-$) is not very high (Table IV).

The dissociation of XN_3 into N_2 and XN via reaction 2 is calculated as exothermic for FN_3, ClN_3, and BrN_3 but endothermic for IN_3 and HN_3. What is the thermodynamic driving force for fragmentation of these compounds? We calculated the reaction energy for dissociation of XN_3 into X_2 and N_2 (reaction 3). After correction for ZPE contributions, rotational and translational degrees of freedom (2.4 kcal/mol), and the work term (1.2 kcal/mol), the reaction enthalpies at room temperature D_0 for reaction 3 have been computed.

$$2XN_3 \rightarrow 3N_2 + X_2 + D_0 \quad (3)$$

Table III shows that reaction 3 is strongly exothermic for all XN_3 molecules. It is interesting to note that the reaction enthalpy of ClN_3, BrN_3, and IN_3 in (3) is nearly the same, while the dissociation of FN_3 and HN_3 is less exothermic. This indicates that the higher tendency of FN_3 to explode[1] is due to the weak FN–N_2 bond (reaction 2).

The calculated reaction enthalpies for reaction 3 may be used to predict theoretically the heats of formation $\Delta H_f°$ at room temperature for the XN_3 molecules. The heats of formation $\Delta H_f°$ of N_2, H_2, F_2, and Cl_2 are zero, while $\Delta H_f°(Br_2) = 11$ kcal/mol and $\Delta H_f°(I_2) = 15.7$ kcal/mol.[38] The calculated $\Delta H_f°$ values

(37) Melius, C. Cited in ref 14c.

(38) Lias, S. G.; Bartmess, J. E.; Liebman, J. F.; Holmes, J. L.; Levin, R. D.; Mallard, W. G. *J. Phys. Chem. Ref. Data* **1988**, *17*, *Suppl. 1*.

Table V. Theoretical Predicted and Experimentally Observed Heats of Formation $\Delta H_f°$ (kcal/mol) for XN_3 Molecules

	HN_3	FN_3	ClN_3	BrN_3	IN_3
MP2/6-31G(d,p)[a]	72.1	82.2	92.8	102.1	103.6
MP2/LANL1DZ+P	68.8	78.9	92.2	97.8	99.7
exptl	71.8[b]				
	71.7[c]				

[a] MP2/HUZ(d) for Br and I. [b] Reference 36a. [c] Reference 38.

for XN_3 and the experimental value for HN_3 are shown in Table V. The agreement between the theoretical and experimental data for the heat of formation of HN_3 is very good. The $\Delta H_f°$ values of the halogen azides increase in the order $FN_3 < ClN_3 < BrN_3 < IN_3$.

4. Electronic Structure of XN_3. The Laplacian distributions for XN_3 molecules at MP2/6-31G(d,p) in the molecular planes are shown in Figure 2. The results of the topological analysis of the wave functions are listed in Table VI.

The Laplacian distribution exhibited in Figure 2 shows regions of electron depletion ($\nabla^2\rho(\mathbf{r}) > 0$, dashed lines) and electron concentration ($\nabla^2\rho(\mathbf{r}) < 0$, solid lines). The solid lines connecting the atomic nuclei are the bond paths.[18] The solid lines separating the nuclei indicate the zero-flux surfaces in the molecular plane. The points where the solid lines are crossing between the atoms are the bond critical points $\mathbf{r}_b$.[18] The shift of $\mathbf{r}_b$ from the "nonpolar" midpoint of a bond A–B may be used as a measure for the effective electronegativity of the atoms. If A and B are identical, the midpoint is simply the half of the calculated interatomic distance. If A and B are different as in case of the X–N bond in XN_3, the sum of the atomic radii a_N and a_X, corrected by the actual interatomic distance r_{XN}, may be used to define the nonpolar midpoint of the X–N bond. If the latter is given by its distance to the nitrogen atom m_N, we define the nonpolar midpoint m_N:

$$m_N = a_N r_{XN}(a_N + a_X)^{-1}$$

m_N = distance of the nonpolar midpoint from atom N

a_N = atomic radius of N in an N–N single bond

a_X = atomic radius of X in an X–X single bond

r_{XN} = calculated interatomic distance X–N

The shift in the bond critical point Δr_b shown in Table VI is then given by the distance between $\mathbf{r}_b$ and m_N for the X–N bond, with positive (negative) values indicating that $\mathbf{r}_b$ is shifted towards the nitrogen (X) atom. A negative (positive) Δr_b for the N_1–N_2 (N_2–N_3) bond means that $\mathbf{r}_b$ is shifted toward N_2 (N_3).

Visual inspection of the contour line diagrams exhibited in Figure 3 shows characteristic differences among the XN_3 molecules, particularly for the X–N bond. The N–H bond in HN_3 is characterized by a continuous area of charge concentration similar to the N–N bonds. The bond critical point of the H–N bond is shifted by –0.056 Å (Table VI) toward the hydrogen atom relative to the nonpolar midpoint of the N–H bond as defined above. Thus, a larger area of the H–N covalent bond is attributed to the nitrogen atom, which can be expected from the electronegativities of N and H. Integration of the atomic basins yields a negative charge of –0.407 e for N_1 and a positive charge of +0.445 e for H (Table VI). A covalent character of the H–N bond is indicated by the large negative value of –0.496 for H_b. The covalent bond order P_{AB}[22] predicts less than a single bond for H–N. The P_{AB} values suggest also that the N_1–N_2 bond is intermediate between a single and a double bond and that the N_2–N_3 bond is nearly a triple bond.

The Laplacian distribution of FN_3 shows that the F–N bond is topologically very different compared with the H–N bond in HN_3. There is a large area of charge depletion in the F–N interatomic region, and the position of the bond critical point $\mathbf{r}_b$ is shifted toward the nitrogen atom by 0.105 Å relative to the nonpolar midpoint (Table VI). This agrees with the higher electronegativity of fluorine than nitrogen. The contour line diagram suggests at first sight that FN_3 might be considered as ionic $F^-N_3^+$. However, integration of the electronic charge over the atomic basins indicates a negative charge of only –0.302 e at fluorine, while N_1 carries a positive charge of +0.245 e. The F–N bond is characterized as covalent by the value of H_b = –0.209 (Table VI). It should be pointed out that the Laplacian distribution is *not* a measure for the absolute concentration of electronic charge; it rather reflects the *curvature* of $\rho(r)$ in three dimensions λ_i (i = 1–3).[18] The curvature along the bond path λ_1 is always positive, while λ_2 and λ_3 are negative in the two directions perpendicular to the bond path. $\nabla^2\rho(\mathbf{r})$ is positive if $|\lambda_1| > (|\lambda_2| + |\lambda_3|)$, and it is negative if $|\lambda_1| < (|\lambda_2| + |\lambda_3|)$. Thus, the Laplacian of the electronic charge is a sensitive probe to show the *differences* in the curvature of the charge distribution of two molecules, but it cannot be used as an *absolute* measure for the charge concentration. It has been shown that the Laplacian distribution for F_2 in the interatomic region is positive (depletion of charge), although the H_b value indicates a strong covalent bond.[21,40] The covalent bond order P_{AB} indicates a F–N single bond in FN_3 (Table VI).

Chlorine is less electronegative than nitrogen, and the contour line diagram of $\nabla^2\rho(\mathbf{r})$ for ClN_3 shows a Cl–N region with a continuous range of charge concentration (Figure 3). The bond critical point $\mathbf{r}_b$ is shifted toward the Cl atom by 0.141 Å relative to the nonpolar midpoint (Table VI). The Cl atom carries a positive charge of +0.118 e, while N_1 has a negative charge of –0.139 e. The Laplacian distribution of the Cl–N bond has a continuous range of charge concentration like HN_3 along the X–N axis, but the value of H_b indicates that the covalency of the Cl–N bond (H_b = –0.131) is less than that of the F–N bond (H_b = –0.209; Table VI). On the other hand, the bond order index P_{AB} of 1.101 for the Cl–N bond is slightly larger than for the F–N bond (Table II), which suggests X–N single bonds in both cases. It seems that the value for H_b (the energy density at the bond critical point $\mathbf{r}_b$) is sensitive to the distance of $\mathbf{r}_b$ from the atomic nuclei. This will become more obvious in the final two examples.

The Laplacian distributions of BrN_3 and IN_3 show large regions of charge depletions around the Br and I nucleuses, respectively. The bond critical point of the X–N bond is shifted toward Br by 0.244 Å in BrN_3 and toward I by 0.324 Å in IN_3 (Table VI). The increase in the polarization is also reflected by the calculated charge distribution, which is +0.210 e (Br) and –0.221 e (N_1) for BrN_3 and +0.353 e (I) and –0.331 e (N_1) for IN_3. The H_b values indicate less covalent contributions for the Br–N bond and particularly for the I–N bond compared with the other X–N bonds. But the bond order indices P_{AB} predict essentially covalent single bonds for Br–N (P_{AB} = 1.049) and I–N (P_{AB} = 0.969). It should be noted that P_{AB} indices are usually quite sensitive to the bond polarity. For example, the P_{AB} value for N_2 is 3.038, but P_{AB} for CO is only 1.509.[22] Thus, the difference in the predicted covalency for the Br–N_3 and I–N_3 bonds between the

(39) The following values for the covalent atomic radii have been used (in Å): H, 0.30; N, 0.70; F, 0.64; Cl, 0.99; Br, 1.14; I, 1.33. They are taken from: Pauling, L. *The Nature of the Chemical Bond*; Cornell University Press: Ithaca, New York, 1960. In case of N and F, the modified values were taken from: Schomaker, V.; Stevenson, D. P. *J. Am. Chem. Soc.* **1941**, *63*, 37.

(40) Another very elegant way of describing the charge concentration in a covalent bond between electronegative atoms has recently been presented by: (a) Schwarz, W. H. E.; Ruedenberg, K.; Mensching, L. *J. Am. Chem. Soc.* **1989**, *111*, 6926. (b) Mensching, L.; Von Niessen, W.; Valtazanos, P.; Ruedenberg, K.; Schwarz, W. H. E. *J. Am. Chem. Soc.* **1989**, *111*, 6933.

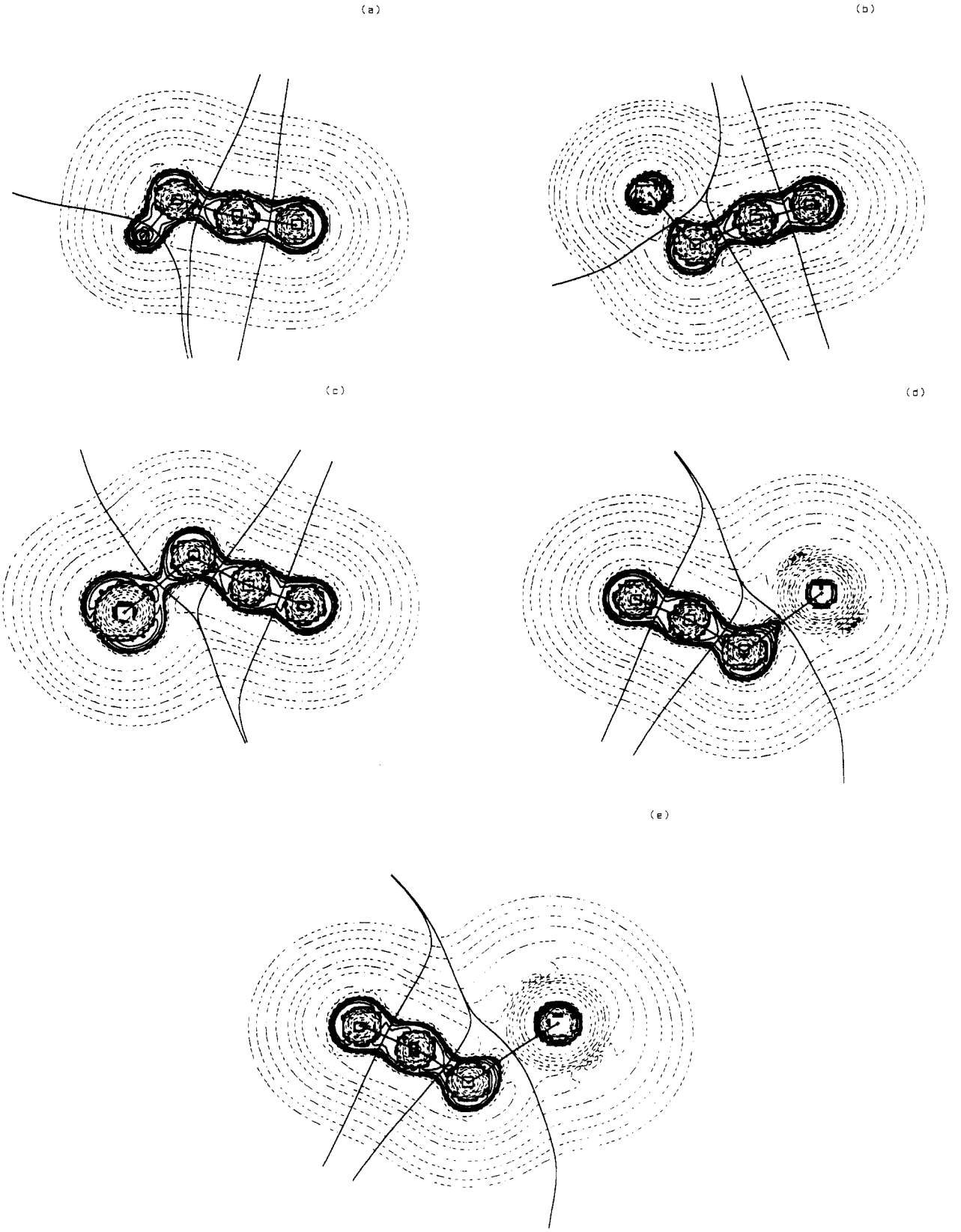

Figure 2. Contour line diagrams of the Laplacian distribution $\nabla^2\rho(\mathbf{r})$ of HN_3 (a), FN_3 (b), ClN_3 (c), BrN_3 (d), and IN_3 (e). Dashed lines indicate charge depletion ($\nabla^2\rho(\mathbf{r}) > 0$), and solid lines indicate charge concentration ($\nabla^2\rho(\mathbf{r}) < 0$). The solid lines connecting the atomic nuclei are the bond paths, and the solid lines separating the atomic nuclei indicate the zero-flux surfaces in the molecular plane.

P_{AB} and H_b values cannot be attributed to the P_{AB} indices being less sensitive to bond polarity.

While the P_{AB} and H_b indices make different predictions for the covalency of the X–N bond, they agree concerning the trend in the N_1–N_2 and N_2–N_3 bonds (Table VI). The N_1–N_2 bond of FN_3, which was calculated to be the weakest among the XN_3 molecules (reaction 2, Table III), has the smallest P_{AB} and H_b values, and HN_3 has the largest bond indices for the N_1–N_2 bond. The P_{AB} and H_b values for the N_1–N_2 bond show the same order as the calculated bond strength. The P_{AB} data predict that the N_1–N_2 bond is always intermediate between a single and a double bond, while the N_2–N_3 bond is nearly a triple bond.

Table VI. Results of the Topological Analysis of XN_3 Molecules at MP2/6-31G(d,p) with HUZ(d) for Br and I: Energy Densities at the Bond Critical Point H_b (Hartree/Å^3), Charge Density at the Bond Critical Point ρ_b (e/Å^3), Distance between the Bond Critical Point and the Nonpolar Midpoint of the Respective Bond Δr_b (Å), Bond Order P_{AB}, and Partial Charges q

HN_3

	$H_{(b)}$	ρ_b	Δr_b	P_{AB}	q(H)	$q(N_1)$	$q(N_2)$	$q(N_3)$
H–N_1	–0.496	0.329	–0.056	0.706	0.445	–0.407	–0.124	0.085
N_1–N_2	–0.552	0.420	–0.076	1.626				
N_2–N_3	–0.837	0.528	0.068	2.820				

FN_3

	$H_{(b)}$	ρ_b	Δr_b	P_{AB}	q(F)	$q(N_1)$	$q(N_2)$	$q(N_3)$
F–N_1	–0.209	0.266	0.105	1.006	–0.302	0.245	–0.098	0.160
N_1–N_2	–0.500	0.403	–0.071	1.451				
N_2–N_3	–0.853	0.538	0.060	2.816				

ClN_3

	$H_{(b)}$	ρ_b	Δr_b	P_{AB}	q(Cl)	$q(N_1)$	$q(N_2)$	$q(N_3)$
Cl–N_1	–0.131	0.189	–0.141	1.101	0.118	–0.139	–0.113	0.136
N_1–N_2	–0.522	0.412	–0.060	1.502				
N_2–N_3	–0.833	0.529	0.064	2.806				

BrN_3

	$H_{(b)}$	ρ_b	Δr_b	P_{AB}	q(Br)	$q(N_1)$	$q(N_2)$	$q(N_3)$
Br–N_1	–0.071	0.136	–0.244	1.049	0.210	–0.221	–0.117	0.125
N_1–N_2	–0.527	0.415	–0.068	1.519				
N_2–N_3	–0.820	0.525	0.064	2.800				

IN_3

	$H_{(b)}$	ρ_b	Δr_b	P_{AB}	q(I)	$q(N_1)$	$q(N_2)$	$q(N_3)$
I–N_1	–0.038	0.099	–0.324	0.969	0.353	–0.331	–0.128	0.104
N_1–N_2	–0.536	0.420	–0.066	1.560				
N_2–N_3	–0.803	0.519	0.064	2.800				

Thus, the electronic structure of the XN_3 molecules given by the topological analysis of the electronic wave functions is as following: The X–N bond is essentially a single bond with a polarity $X^{\delta-}$–$N^{\delta+}$ for FN_3 and $X^{\delta+}$–$N^{\delta-}$ for HN_3, ClN_3, BrN_3, and IN_3. The N_1–N_2 bond has a covalent bond order which is intermediate between a single and a double bond. The bond order indices P_{AB} and H_b for the N_1–N_2 bond decrease with the same sequence as the calculated bond strength. The N_2–N_3 bond has nearly a triple bond as indicated by the P_{AB} values. The partial charge is always slightly negative at N_2 and slightly positive at N_3.

5. Summary. The halogen azides XN_3 are theoretically predicted to have trans-bent (C_s) geometries with a nearly constant N_3 bond angle of ~172° and XNN angles which increase from ~103° for FN_3 to ~111° for IN_3. The agreement between the calculated geometries at MP2/6-31G(d,p) and MP2/LANL1DZ+P and the experimental values for HN_3, FN_3, and ClN_3 is satisfactory. The X–N bond lengths for BrN_3 and IN_3, which have not been measured yet, are predicted as ~1.92 Å for Br–N_3 and ~2.11 Å for I–N_3. A systematic comparison of the experimental vibrational frequencies and the calculated data using scaling factors suggests that in case of BrN_3 and IN_3 some assignments of the experimental spectra are probably incorrect.

The X–N_3 bond strength of the XN_3 molecules is predicted to show the sequence H ≫ F > Cl > Br > I; i.e., FN_3 has the strongest X–N_3 bond and IN_3 has the weakest. Dissociation of XN_3 into XN + N_2 is predicted as exothermic for FN_3, ClN_3, and BrN_3, but endothermic for IN_3 and HN_3. The high tendency of FN_3 to explode is traced back to the weak FN–N_2 bond. The calculated H–N_3 and HN–N_2 bond dissociation energies and the heat of formation $\Delta H_f°$ for HN_3 are in very good agreement with experimental values.

The topological analysis of the electronic wave functions shows that the X–N bond is essentially a single bond with a polarity $X^{\delta-}$–$N^{\delta+}$ for FN_3 and $X^{\delta+}$–$N^{\delta-}$ for ClN_3, BrN_3, and IN_3. The covalent bond order index P_{AB} indicates that the N_1–N_2 bond in XN_3 is intermediate between a single and a double bond and that the N_2–N_3 bond has nearly a triple bond. The partial charge is always slightly negative at N_2 and slightly positive at N_3.

Acknowledgment. Stimulating discussions with Prof. K. Dehnicke are gratefully acknowledged. We thank A. Gobbi for his technical assistance with the topological analysis. This work has been financially supported by the Fonds der Chemischen Industrie and the Deutsche Forschungsgemeinschaft. Additional support was provided by the computer companies Convex and Silicon Graphics. Additional computer time was given by the HLRZ Jülich.

Registry No. FN_3, 14986-60-8; ClN_3, 13973-88-1; BrN_3, 13973-87-0; IN_3, 14696-82-3; HN_3, 7782-79-8.